Molecular Cancer Therapeutics

Urolithin A, a Novel Natural Compound to Target PI3K/AKT/mTOR Pathway in Pancreatic Cancer

Tulasigeri M. Totiger[1], Supriya Srinivasan[1], Venkatakrishna R. Jala[2], Purushottam Lamichhane[1], Austin R. Dosch[1], Alexander A. Gaidarski III[1], Chandrashekhar Joshi[1], Shobith Rangappa[3], Jason Castellanos[4], Praveen Kumar Vemula[5], Xi Chen[6], Deukwoo Kwon[6], Nilesh Kashikar[7], Michael VanSaun[1], Nipun B. Merchant[1], and Nagaraj S. Nagathihalli[1]

Abstract

Pancreatic ductal adenocarcinoma (PDAC) is an aggressive malignancy and is highly resistant to standard treatment regimens. Targeted therapies against *KRAS*, a mutation present in an overwhelming majority of PDAC cases, have been largely ineffective. However, inhibition of downstream components in the KRAS signaling cascade provides promising therapeutic targets in the management of PDAC and warrants further exploration. Here, we investigated Urolithin A (Uro A), a novel natural compound derived from pomegranates, which targets numerous kinases downstream of KRAS, in particular the PI3K/AKT/mTOR signaling pathways. We showed that treatment of PDAC cells with Uro A blocked the phosphorylation of AKT and p70S6K *in vitro*, successfully inhibited the growth of tumor xenografts, and increased overall survival of Ptf1a$^{Cre/+}$;LSL-Kras$^{G12D/+}$;Tgfbr2$^{flox/flox}$ (PKT) mice compared with vehicle or gemcitabine therapy alone. Histologic evaluation of these Uro A–treated tumor samples confirmed mechanistic actions of Uro A via decreased phosphorylation of AKT and p70S6K, reduced proliferation, and increased cellular apoptosis in both xenograft and PKT mouse models. In addition, Uro A treatment reprogrammed the tumor microenvironment, as evidenced by reduced levels of infiltrating immunosuppressive cell populations such as myeloid-derived suppressor cells, tumor-associated macrophages, and regulatory T cells. Overall, this work provides convincing preclinical evidence for the utility of Uro A as a therapeutic agent in PDAC through suppression of the PI3K/AKT/mTOR pathway.

Introduction

Pancreatic ductal adenocarcinoma (PDAC) is the third leading cause of cancer-related death in the United States with a 5-year survival rate below 9%. The prevalence of distant metastases and chemotherapeutic resistance are hallmarks of the disease which largely account for its dismal prognosis (1, 2). Current standard-of-care drug regimens including gemcitabine, FOLFIRINOX, and nab-paclitaxel/gemcitabine have shown limited clinical efficacy and are often poorly tolerated in patients due to toxic side effects (3). Hence, there is a desperate need to develop novel therapeutic approaches which reduce PDAC tumor burden without producing significant off-target effects.

Natural compounds have garnered increasing attention among the scientific community for their low cost, high bioavailability, and limited toxicity compared with synthetic pharmaceutical agents (4). Mounting evidence suggests that many of these compounds possess intrinsic antioxidant, anti-inflammatory, and antitumor activities (5). In fact, a growing number of FDA-approved anticancer agents are derived from either naturally occurring compounds or their derivatives (5, 6). Interestingly, population-based epidemiologic studies have shown a strong inverse correlation between consumption of berries, such as black raspberries, pomegranates, and strawberries, and incidence of PDAC (6, 7). Although the mechanism is poorly understood, it has been postulated that this effect is due to the high concentration of ellagitannins present in these foods. Ellagitannins are hydrolyzed in the gut to release ellagic acid (EA), a compound which inhibits multiple oncogenic pathways which are activated in PDAC such as COX-2, NF-κB, Notch, and Wnt signaling. Preclinical studies have shown that targeted blockade of these pathways by EA is successful in reducing epithelial–mesenchymal transition, angiogenesis, fibrosis, and pancreatic stellate cell activation in PDAC (8, 9). Despite these promising developments, EA is unfortunately poorly absorbed within the human gut, limiting its efficacy as a therapeutic agent. However, EA is metabolized into a number of downstream compounds through microbial processing, including the urolithin A, B, and C (10, 11). Of these, Urolithin

[1]Department of Surgery, University of Miami Miller School of Medicine, Sylvester Comprehensive Cancer Center, Miami, Florida. [2]Department of Microbiology and Immunology, University of Louisville, Louisville, Kentucky. [3]Adichunchanagiri Institute for Molecular Medicine, AIMS, Karnataka, India. [4]Department of Surgery, Vanderbilt University School of Medicine, Nashville, Tennessee. [5]Institute for Stem Cell Biology and Regenerative Medicine (inStem), Bangalore, Karnataka, India. [6]Department of Public Health, University of Miami Miller School of Medicine, Miami, Florida. [7]Department of Pathology, University of Colorado, Denver, Colorado.

Note: Supplementary data for this article are available at Molecular Cancer Therapeutics Online (http://mct.aacrjournals.org/).

T.M. Totiger and S. Srinivasan contributed equally to this article.

Corresponding Author: Nagaraj S. Nagathihalli, University of Miami, Miller School of Medicine, Sylvester Comprehensive Cancer Center, 1550 NW 10th Ave, FOX140, Miami, FL 33136. Phone: 361-720-9347; Fax: 305-243-2810; E-mail: nnagathihalli@med.miami.edu

doi: 10.1158/1535-7163.MCT-18-0464

A (Uro A) exhibits potent antioxidant and anti-inflammatory properties, suggesting it may be the dominant compound which is responsible for the intrinsic antitumor activity of EA (12, 13). These data suggest that although dietary ingestion of EA is unable to produce therapeutic levels, direct oral administration of Uro A may be a promising target in the treatment of PDAC due to its improved bioavailability and potent antitumor effects. Furthermore, preclinical models have demonstrated that Uro A is well tolerated and does not elicit any adverse toxic effects at clinically relevant doses (11).

Despite their limited efficacy, gemcitabine- and 5-FU–based adjuvant chemoradiation has been considered the standard of care for PDAC. To date, the addition of targeted molecular therapies to these cytotoxic compounds has failed to show any significant improvement in improving overall survival (OS) in PDAC (14, 15), presumably due to redundant signaling pathways and feedback loops within tumor cells (12). Furthermore, overcoming these resistance mechanisms by combining multiple inhibitors is not feasible due to cumulative toxicity. As such, single chemotherapeutic agents that are both well tolerated and able to target multiple kinase pathways simultaneously present novel targets in the treatment of PDAC. Uro A has been shown to downregulate multiple tumor pathways in colon, prostate, and bladder cancer through downregulation of several oncogenes such as Kras and c-myc, upregulation of tumor-suppressor genes such as FGFR2 and EGFR, and modulation of enzyme activity, such as CYP1 (13). Despite the promising effects seen in treating other malignancies, the anticancer effect of Uro A in PDAC is currently unknown (8, 9).

We hypothesized that Uro A exerts its antitumor effects through inhibition of multiple protumorigenic pathways in PDAC. Our results clearly demonstrated that Uro A downregulated the oncogenic PI3K/AKT/mTOR signaling pathway, induced cell-cycle arrest, and increased apoptosis. Uro A successfully attenuated tumor growth in both tumor xenografts and genetically engineered mouse models *in vivo* by not only disrupting PI3K/AKT signaling, but also inducing significant changes within the immunosuppressive microenvironment of PDAC.

Materials and Methods

Cell lines and drugs

The human PDAC cell lines MiaPaCa2, PANC1, AsPC1, CFPAC1, Capan1, Capan2, SW1990, HPAC, and BxPC3 were obtained from the American Type Culture Collection (ATCC). The K8484 ($Pdx1a^{Cre/+}$; $LSL\text{-}KRAS^{G12D/+}$; $p53^{R172H/+}$) cell line was obtained from Dr. Tuveson (Cold Spring Harbor Laboratory). All tumor cells were maintained according to the ATCC guidelines. ATCC cell lines were characterized and verified free of Mycoplasma contamination, tested by Hoechst DNA stain (indirect) and agar culture (direct) methods. Cell authentication was performed by using short tandem repeat DNA profiling (latest date: June 16, 2016, and July 21, 2017) and cell lines tested negative for *Mycoplasma* via Genetica cell line testing using eMYCO plus kit (iNtRON Biotechnology). Cells with relatively low-passage numbers (< 20) were used in the study.

Uro A synthesis and the structure of the compound were as detailed previously (16), and gemcitabine was purchased from Eli Lilly and Company. AKT activators SC79 and IGF-1 were purchased from Sigma Aldrich and R&D systems, respectively. AKT inhibitor MK2206 was purchased from Selleckem.

Western blotting

Cell lysis and Western blotting were done as previously described (17). Briefly, cells were washed, lysed, and removed from culture dishes by scraping after treatment. Cell lysis was performed using RIPA buffer (0.1% SDS, 50 mmol/L Tris·HCl, 150 mmol/L NaCl, 1% NP-40, and 0.5% Na deoxycholate) with protease inhibitor cocktail (Sigma) and PhosSTOP phosphatase inhibitor (Roche). Lysates were sonicated and centrifuged at 10,000 *g* for 15 minutes at 4°C to collect supernatant. The protein concentration of the lysate was determined by Bio-Rad protein assay kit (Bio-Rad). Per lane, 35 μg of whole-cell lysate was separated on NuPAGENovex 4%–12% Bis-Tris Gels and transferred on iBlot transfer stack and PVDF membranes using iBlot dry blotting transfer system (Life Technologies). For immunodetection, membranes were incubated with antibodies listed in Supplementary Table S1. The membranes were subsequently incubated with corresponding secondary anti-mouse or anti-rabbit secondary antibodies conjugated with horseradish peroxidase (Jackson ImmunoResearch). Finally, the immunoreactive bands were developed with Pierce ECL Western Blotting Substrate (Thermo Scientific) and recorded on blue basic autoradiography film (Bioexpress).

The human tyrosine kinase array was purchased from R&D Systems (Cat#: ARY003B) and used according to the manufacturer's recommended conditions. Both immunoblots and array intensity were then quantified using Image J image analysis software. Statistical analysis was performed using Prism software (Graphpad Software Inc.).

Cell viability assay (MTT)

PDAC cells were seeded at a concentration of 1×10^4 cells per well in 96-well plates. Twenty-four hours after seeding, the attached cells were treated with DMSO or Uro A (0–100 μmol/L) for 48 hours, and cell viability was determined by MTT assay (Sigma) according to the manufacturer's direction. IC_{50} was calculated using Prism software (Graphpad Software Inc.). Each condition was assayed in triplicate.

Apoptosis assay

Apoptosis was assessed by flow cytometric detection of phosphotidyl serine externalization using the FITC Annexin V Apoptosis Detection Kit II (BD Biosciences). MiaPaCa2 cells were treated with Uro A for 24 hours. The cells were then trypsinized gently, washed twice with cold PBS, resuspended in 1X binding buffer, and then incubated with 5 μL of FITC Annexin V and 5 μL of propidium iodide (PI). After incubation for 15 minutes at room temperature (25°C) in the dark, 400 μL of 1X binding buffer was added, and each tube was analyzed within 1 hour using the FACSCalibur flow cytometer (BD Biosciences). The percentage of cells present in each compartment was measured and analyzed with Cell Quest software (BD Biosciences).

Wound-healing assay

Cells were treated with mitomycin C (0.5 μg/mL) for 4 hours prior to wounding. Wounds were made across the cell monolayer by a sterile pipette tip. After wounding, BxPC3 and MiaPaCa2 cells were treated with DMSO or Uro A (0–50 μmol/L) for 36 hours. Phase contrast images were taken. After every 12 hours of wound-healing study, the cells were washed and treated with Uro A or DMSO for up to 36 hours and observed for recovery after wounding.

Cell-cycle analysis

Cells were harvested, stained, washed, and resuspended as described before (18). Cell fluorescence signals were determined using a FACS Caliber flow cytometer and analyzed with its Cell Quest software.

Xenograft models

Athymic nude mice—Foxn1 *nu/nu* (4–5 weeks old)—were purchased from Harlan Sprague Dawley, Inc. Subcutaneous tumors were established by injecting 2×10^6 MiaPaCa2 or PANC1 cells into the flank of a 6-week-old Fox1-*nu/nu* mouse ($n = 5$ in each group) as previously detailed (18). MiaPaCa2 and PANC1 were chosen because they harbor mutations typical of human pancreatic cancer (19). Uro A (20 mg/kg/daily) daily (5 days/week) by oral gavage was initiated when the subcutaneous tumors reached 200 to 250 mm^3 size. Uro A or vehicle (10% glucose in water) was administered by oral gavage for 33 (MiaPaCa2) and 42 (PANC1) days, and the tumor volume was measured weekly. The subcutaneous tumor volume and percent body weight change were recorded as previously described (18). Growth curves for tumors were plotted as the mean volume ± SD of tumors for mice from each group. At the end of the study, animals were sacrificed, and primary tumors were removed for further analysis.

Mice

Ptf1a$^{Cre/+}$;*Tgfbr2*$^{flox/flox}$ and *LSL-Kras*$^{G12D/+}$;*Tgfbr2*$^{flox/flox}$ mice were provided by Dr. Hal Moses (Vanderbilt University Medical Center, Nashville, TN). These 2 lines were intercrossed to generate *Ptf1a*$^{Cre/+}$;*LSL-Kras*$^{G12D/+}$;*Tgfbr2*$^{flox/flox}$ (PKT) mice on a C57Bl/6 background. Genotyping of alleles was performed using oligonucleotide primers as described previously (18, 20).

Treatment of PKT mice

PKT mice were treated with vehicle or Uro A and/or gemcitabine. Mice in the Uro A (20 mg/kg/day) arm received treatment by oral gavage 5 days/week and received twice-weekly intraperitoneal injections of gemcitabine (20 mg/kg), starting at 4 weeks of age. Mice were euthanized and dissected after 3 weeks unless they were part of the survival arm. Due to the irregularity of the tumor dimensions, size was determined by weighing the entire tumor. Tumor tissue was processed for further IHC examination. OS was determined by the log-rank analysis using statistical software package R (version 3.3.2).

Immunohistochemistry

Tissues were fixed and immunostained using antibodies against Ki67 and cleaved caspase-3 (Supplementary Table S1). Stained tissues were evaluated by an expert pathologist (N. Kashikar). Immunostained slides were imaged using Leica microscope (Leica Microsystems, Inc.) and quantified using Image J. Images were adjusted to exclude areas containing obvious histologic artifacts, such as tissue folds or nonorganic material, from the digital image. Calculated percentage of positive cells stained relative to total area was analyzed by applying a scale for relative intensity and was reported as relative expression of protein staining.

Flow cytometry

PKT mouse pancreas were minced and digested with 1 mg/mL Collagenase P (Roche) and 2 mg/mL Collagenase IV (Gibco) for 30 minutes at 37°C. The dissociated tissue was then filtered to remove the large chunks, washed with PEB, and refiltered to obtain single-cell suspensions. Single-cell suspensions were prepared for flow cytometry by staining for regulatory T cells (Treg) and myeloid-derived suppressor cells (MDSC) with the following antibodies: CD45 PE-Cy7, CD3 APC, CD4 AF700, CD8 PerCpCy5.5, Foxp3 PE, CD25 APC-Cy7, CD11b AF700, Gr1 FITC, and Live/Dead Aqua (Supplementary Table S2).

Statistical analysis

Descriptive statistics were calculated using Microsoft Excel and Prism software (Graphpad Software Inc.). Results are shown as values of mean ± SD unless otherwise indicated. Statistical analyses of IHC data were performed using the Student t test with $P < 0.05$ taken as significant, except where indicated otherwise. Statistical analyses of PKT tumor weight data were performed using the ANOVA followed by Tukey's multiple comparisons test to determine P values.

Statistical analysis for Figs. 3B and C, and 4C was adjusted using area under the growth curve (aAUC) approach (21). P values were obtained from permutation test to compare aAUCs of tumor growth curves between groups. The Kaplan–Meier survival analysis was performed, and survival differences between groups were assessed with the log-rank test. All statistical analyses were performed using statistical software package R (version 3.3.2).

Study approval

All experiments were performed in compliance with the regulations and ethical guidelines for experimental and animal studies of the Institutional Animal Care and Use Committees at the Vanderbilt University Medical Center and the University of Miami (#15-057 and #18-081).

For additional experimental procedures, please refer to Supplementary Materials and Methods.

Results

Uro A treatment inhibits PDAC cell proliferation and migration, and enhances apoptosis

Nine PDAC cell lines were tested for sensitivity to Uro A *in vitro* using a cell viability assay (Fig. 1A). IC_{50} values of Uro A for these cell lines were determined 48 hours after treatment (Supplementary Table S3). Briefly, Capan1 and HPAC (IC_{50}, 10.23–10.28 μmol/L) displayed the most sensitive response, and CFPAC1 and AsPC1 (IC_{50}, 40.39–62.28 μmol/L) showed the least sensitivity to Uro A treatment. MiaPaCa2, BxPC3, and PANC1 (IC_{50}, 15.8–24.8 μmol/L) cell lines displayed intermediate sensitivity and hence were chosen to ascertain the antineoplastic effects of Uro A in further experiments. Other Uro derivatives such as Uro B and C, on the other hand, failed to exhibit growth-inhibitory effects as effectively as Uro A (Supplementary Fig. S1A and S1B). Previous studies have established that Uro A doses up to 100 μmol/L are clinically tolerated (22, 23).

In order to investigate the mechanism of PDAC growth inhibition by Uro A, we examined its effect on the inducing apoptosis (Fig. 1B; Supplementary Fig. S2A) and/or cell-cycle alterations by assessing sub-G_0, G_1, S, and G_2 populations (Supplementary Fig. S2B). Uro A treatment resulted in a dose-dependent increase in both the sub-G_0 (PI positive) and apoptotic (Annexin V–positive/PI-negative) populations at concentrations at or above 25 μmol/L, suggesting that Uro A

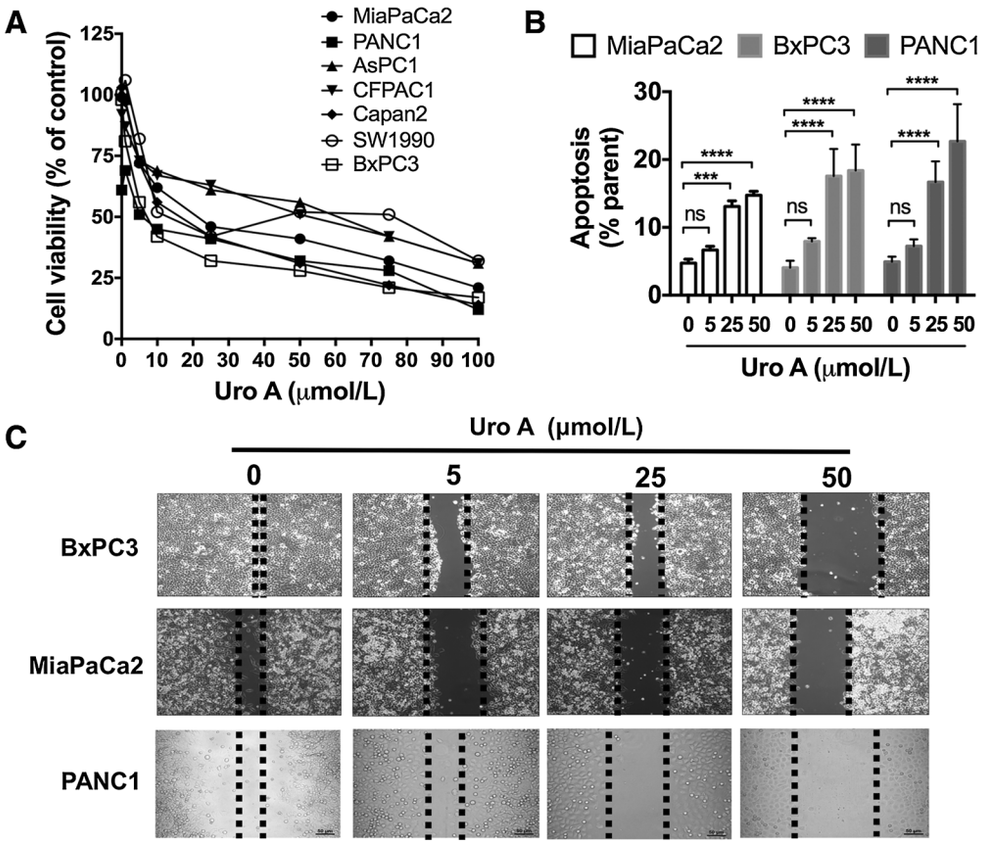

Figure 1.

Uro A treatment attenuates PDAC cell viability and migration and enhances apoptosis. **A,** Relative cell viability in MiaPaCa2, PANC1, AsPC1, CFPAC1, Capan2, SW1990, and BxPC3 cells upon treatment with Uro A (0–100 μmol/L) for 48 hours was assessed using MTT assay. **B,** MiaPaCa2, BXPC3, and PANC1 cells were treated with Uro A (0–50 μmol/L) for 24 hours in a dose-dependent manner, stained with Annexin V–FITC and PI, and analyzed for apoptosis (Annexin-positive and PI-negative) using flow cytometry. **C,** Wound-healing assay to assess the effect of Uro A (0–50 μmol/L) treatment on cell motility of BxPC3, MiaPaCa2, and PANC1 cells 36 hours after treatment. ***, $P < 0.001$; ****, $P < 0.0001$; and ns, $P > 0.05$.

leads to PDAC cell death. In addition, we tested migratory potential of PDAC cells by using a wound-healing assay wherein we noted a concentration-dependent reduction in cell migration in response to Uro A (Fig. 1C), which correlated with the cell line sensitivity to Uro A treatment measured using a cell viability assay (Supplementary Table S3).

Uro A treatment downregulates PI3K/mTOR pathway in PDAC cells

To explore the regulatory molecular mechanisms underlying the growth-inhibitory effects of Uro A in human PDAC cells, we first screened for alterations in the inactivation of multiple cellular kinase pathways in MiaPaCa2 cells exposed to Uro A (25 μmol/L) for 3 hours (Supplementary Fig. S3). The phosphokinase array data revealed a significant decrease in the phosphorylation of AKT (T308) and p70S6K (T421/S424) upon Uro A treatment. AKT and p70S6K enhance proliferation, inhibit apoptosis, and promote invasion and metastasis in PDAC (24). AKT activity is dependent on phosphorylation at two sites: T308, which is activated by phosphoinositide-dependent kinase-1 (PDK1), and S473, which is activated by PI3K and mTORC2 complex composed of mTOR, rictor, and Sin1 (25, 26). AKT activation mediated through phosphorylation at T308 and/or S473 further leads to regulation of p70S6K through mTORC1 complex. In addition, mTOR is known to regulate p70S6K. Combined targeting of the PI3K/AKT/mTOR pathway is necessary to prevent the reactivation of AKT through mTORC2. To validate the results obtained from our kinase array, we exposed human PDAC cells (MiaPaCa2, BxPC3, and PANC1; Fig. 2A) and mouse KPC cells (K8484; Fig. 2B) to different doses of Uro A (0–100 μmol/L) and immunoblotted for phospho-AKT and phospho-p70S6K levels. Our results confirmed that Uro A treatment induces a significant dose-dependent reduction in both pAKT and pP70S6K expressions in PDAC cell lines (Fig. 2A and B).

Subsequent studies were performed to determine whether AKT was a critical mediator of the antitumor effects of Uro A. BxPC3 cells were treated with known activators of AKT such as SC79 (Fig. 2C, top plot) and IGF-1 (Fig. 2C, bottom plot), with or without Uro A and blotted for pAKT. Cells treated with SC79 or IGF-1 showed a prominent activation of AKT and Uro A treatment significantly reduced SC79 or IGF-1 induced pAKT levels. To determine whether IGF-1 induced cell proliferation through an AKT-dependent mechanism, we treated control or AKT knockdown BxPC3 cells with IGF-1 (Supplementary

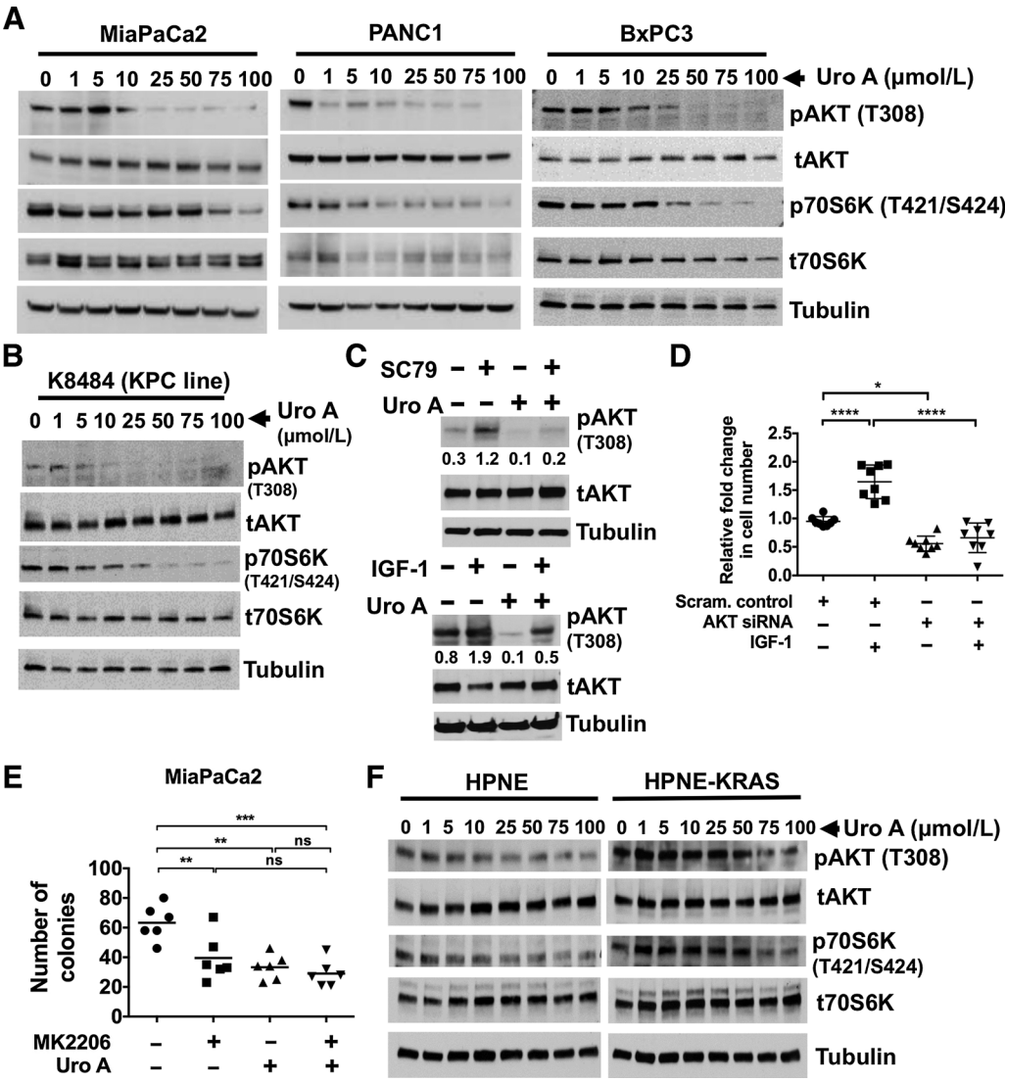

Figure 2.

Uro A treatment downregulates PI3K/AKT/P70S6K pathway in PDAC cells. **A,** Western blots demonstrating dose-dependent phosphorylation of AKT and p70S6K in primary human PDAC cell lines MiaPaCa2, PANC1, and BxPC3 upon Uro A (0–100 μmol/L) treatment for 3 hours. **B,** Cell line (K8484) established from KPC mouse was treated with Uro A (0–100 μmol/L) for 3 hours. Western blot demonstrating dose-dependent decrease in the levels of phosphorylation of AKT and p70S6K in K8484 cell line upon Uro A treatment. Tubulin was used as Western blots loading control. **C,** BxPC3 cells were treated with SC79 (10 μmol/L; top) or IGF-1 (50 ng/mL; bottom) for 3 hours with activated AKT. The densitometry analyses of pAKT normalized to total AKT protein were shown. Cells treated with Uro A (25 μmol/L) show a significant reduction in the pAKT levels when compared with SC79 or IGF-1–alone–treated cells. **D,** IGF-1 (50 ng/mL) exposure to AKT knockdown BxPC3 cells shows a significant reduction in the cell proliferation when compared with scrambled control cells treated with IGF-1 alone. **E,** MiaPaCa2 cells treated with either MK2206 or Uro A showed decreased number of colonies. Combination of MK2206 (1 μmol/L) and Uro A did not affect further the number of colonies when compared with either MK2206 or Uro A treatment. **F,** Western blots demonstrating dose-dependent phosphorylation of AKT and p70S6K in primary human normal pancreas cell lines HPNE and HPNE-KRAS upon Uro A (0–100 μmol/L) treatment for 3 hours. *, $P < 0.05$; **, $P < 0.01$; ***, $P < 0.001$; ****, $P < 0.0001$; ns, $P > 0.05$.

Fig. S4A; Fig. 2D). With the addition of IGF-1, BxPC3 control cells significantly increased cell proliferation compared with IGF-1 treatment of AKT knockdown cells. Next, AKT knockdown cells showed a significant reduction in IGF-1–mediated cell proliferation in comparison with its corresponding scrambled control cells treated with IGF-1. These results confirm that IGF-1–induced activation of AKT regulates cell proliferation in PDAC cells. Furthermore, Uro A treatment also downregulated PDK1 (an upstream target of AKT) as well as pGSK3β and p4E-BP1 (downstream targets of AKT), thereby suggesting that Uro A effectively inhibits the PDK1/AKT/mTOR pathway (Supplementary Fig. S4B). Further, treatment of MiaPaCa2 cells with the AKT inhibitor MK2206 or Uro A resulted in an attenuated number of colonies (Fig. 2E). The combined treatment with MK2206 and Uro A did not produce further inhibition when compared with either MK2206 or Uro A single treatments. These results demonstrate that Uro A elicits its anticancer effects on PDAC proliferation that are consistent with AKT inhibition

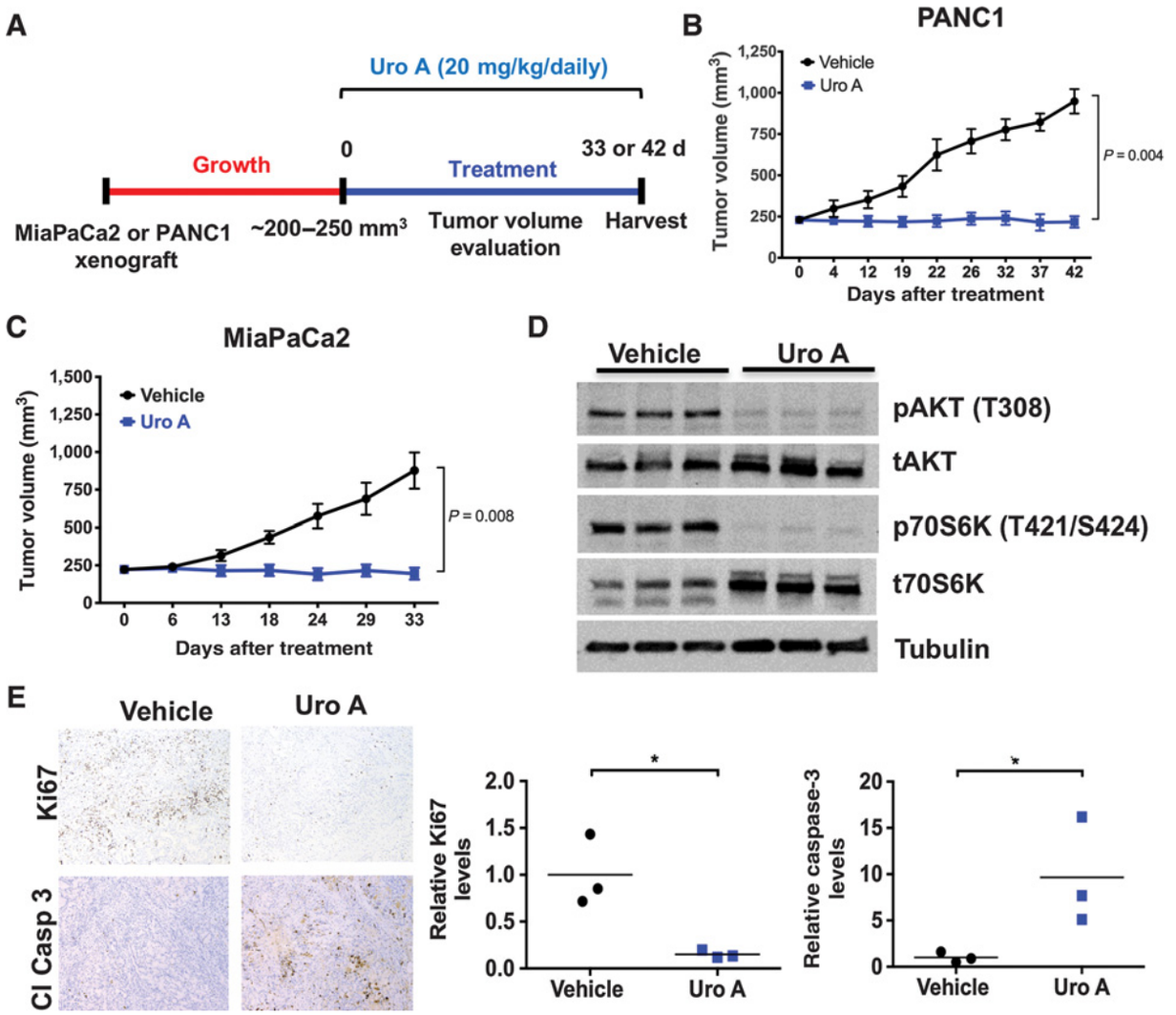

Figure 3.

Uro A treatment decreases the growth of pancreatic tumor xenograft. **A,** Experimental design for Uro A treatment in PANC1 and MiaPaCa2 xenograft mouse model. **B** and **C,** PANC1 (**B**) and MiaPaCa2 (**C**) cells were s.c. injected onto the flank of Fox1-nu/nu mice until tumor volume reached 200 to 250 mm^3. The xenograft tumors were further treated with Uro A (20 mg/kg/daily) or vehicle (10% glucose in water) by oral administration for 42 (**B**) or 33 (**C**) days, and their respective volumes were measured daily ($n = 5$). Both PANC1 and MiaPaCa2 xenografts exhibited significantly reduced tumor growth with Uro A treatment in comparison with corresponding vehicle-treated xenografts. By repeated measures *t* test, PANC1 achieved significance at 22 days of treatment and MiaPaCa2 at 24 days. Growth trajectory was significantly different by linear regression ($P < 0.0001$ for both cell lines), and treatment was statistically significant by two-way ANOVA for PANC1 ($P = 0.0002$) and MiaPaCa2 ($P = 0.0024$). **D,** Western blot demonstrating levels of pAKT and p70S6K in corresponding resected vehicle and Uro A–treated MiaPaCa2 xenograft tissues harvested 33 days after treatment. **E,** Representative Ki67 and cleaved caspase-3 staining of vehicle or Uro A–treated MiaPaCa2 flank xenograft tissues (left). Quantification of Ki67 and cleaved caspase-3 staining data obtained from resected vehicle or Uro A–treated MiaPaCa2 flank xenograft tissues (right). *, $P < 0.05$.

(Supplementary Fig. S4C). Interestingly, Uro A displayed only a mild effect on pAKT and pP70S6K expression in normal epithelial cell lines HPNE and HPNE-KRAS (Fig. 2F; Supplementary Fig. S5), thereby suggesting potential for cancer cell selectivity of Uro A.

Uro A treatment suppresses the growth of pancreatic tumor xenografts in mice

After characterizing the efficacy of Uro A in PDAC cell lines, we proceeded to test this treatment *in vivo* using a mouse xenograft model (Fig. 3A). PANC1 (Fig. 3B) and MiaPaCa2 (Fig. 3C) xenografts were generated via subcutaneous flank injection of PDAC tumor cells into athymic nude mice. These xenograft-bearing mice were then treated with either Uro A or vehicle (Fig. 3A). Immunoblotting of Uro A–treated MiaPaCa2 xenograft tumor lysates demonstrated significant inhibition of AKT and p70S6K phosphorylation (Fig. 3D). Uro A–treated xenograft mice exhibited significantly reduced tumor growth in comparison with corresponding vehicle-treated xenograft mice (Fig. 3B and C). IHC performed on xenograft specimens revealed a significant decrease

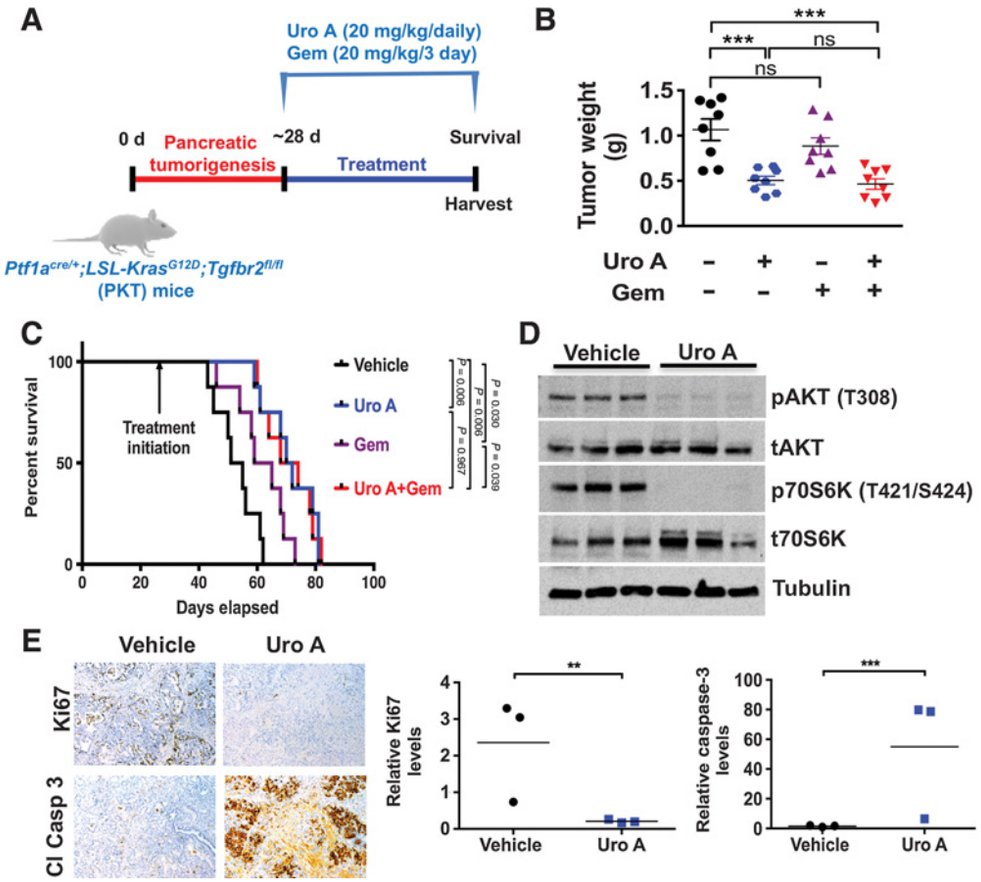

Figure 4.

Uro A treatment improves survival of PKT mice. **A,** Experimental design for Uro A (20 mg/kg/daily), gemcitabine (Gem; 20 mg/kg/3 day), or Uro A+Gem treatment in PKT mice starting at 4 weeks of age ($n = 8$ per group). **B,** Tumor weight in the Uro A or Uro A+Gem-treated mice was significantly decreased compared with vehicle-treated controls. **C,** Kaplan–Meier survival analysis shows significantly improved OS with Uro A (median 71 days) or Uro A+Gem (median 71 days) compared with vehicle control (median 53 days). The log-rank test was used to compare groups, with Bonferroni correction applied to pairwise comparisons to account for multiple comparisons. **D,** Western blot analysis of whole tumor lysates demonstrated decreased expression of pAKT and p70S6K in mice treated with Uro A compared with vehicle-treated mice. **E,** Representative proliferation (Ki67 staining) and apoptosis (cleaved caspase-3) staining of resected pancreata obtained from Uro A–treated PKT mice (left plot). Proliferation was significantly decreased, and apoptosis was significantly increased with Uro A treatment when compared with vehicle-treated mice (right plot). **, $P < 0.01$; ***, $P < 0.001$; and ns, $P > 0.05$.

in proliferation and a significant increase in apoptosis, as measured by Ki67 and cleaved caspase-3, respectively (Fig. 3E). Overall, Uro A treatment was well tolerated by murine hosts and did not have any negative impact on body weight throughout treatment (Supplementary Fig. S6A and S6B).

Uro A inhibits tumor growth and improves survival in *PKT* mice

To further explore the effect of Uro A treatment on PDAC tumor growth, we utilized the genetically engineered PKT mouse model. These mice develop autochthonous PDAC with full penetrance that reliably recapitulates the clinical and histopathologic features of the human disease. They consistently develop PanIN lesions at 3.5 weeks of age which progresses to invasive cancer by 4.5 weeks of age. Median OS of PKT mice is consistently around 59 days (18, 20). Treatment regimens consisting of either Uro A and/or gemcitabine were initiated at 4 weeks of age, and mice were followed until moribund for survival (Fig. 4A). Tumor weight was significantly reduced in all treatment groups compared with vehicle-treated mice (Fig. 4B). Both monotherapy and combined Uro A/gemcitabine treatments were well tolerated without appreciable toxicity, as evidenced by normal body weight (Supplementary Fig. S6C). Similarly, all treatment groups had improved survival compared with vehicle-treated mice (median OS = 53 days; Fig. 4C). However, only Uro A (OS = 71 days) and Uro A + gemcitabine (OS = 71 days) groups attained statistical significance for OS by the Mantel–Cox log-rank test with Bonferroni-adjusted *P* value. Furthermore, combined administration of Uro A and gemcitabine did not provide any additional survival advantage over single-agent administration of Uro A, nor did it provide statistically significant advantage of single-agent treatment with gemcitabine (OS = 62 days). Immunoblot analyses of whole-tumor lysates showed decreased activation of AKT and p70S6K, reduced proliferation, and enhanced cellular apoptosis with Uro A treatment (Fig. 4D and E), consistent with the findings seen *in vitro* and in xenograft tumor models. Taken together, these data show that Uro A is an effective single-agent therapy that reduces

tumor burden *in vivo* through significant reduction in tumor cell proliferation and an increase in apoptosis. Overall, Uro A is more effective than gemcitabine in improving OS.

Improved therapeutic response to Uro A treatment is associated with a reduction in immunosuppressive tumor-associated macrophages and Tregs in PKT mice

The immunosuppressive tumor microenvironment (TME) of PDAC is a substantial deterrent to achieving a durable therapeutic response (27). MDSCs, tumor-associated macrophages (TAMs), and Tregs are the major components of this immunosuppressive milieu (28), as these cell types have been shown to promote systemic T-cell dysfunction that allows PDAC tumors to escape immune detection. Tregs are critically dependent on the transcription factor FoxP3 (29), and TAMs are primarily identified as the F4/80$^+$ population (30). Signaling through the AKT pathway and its corresponding downstream target p70S6K has been shown to play a critical role in regulating this process (31). PKT tumor samples were analyzed for F4/80 and FoxP3 by IHC after treatment with Uro A or vehicle alone. Our results demonstrated that Uro A treatment significantly reduced the detection of tumor-infiltrating F4/80-positive TAMs as well as the presence of FoxP3-positive Tregs without decreasing the overall CD3-positive T-cell staining (Fig. 5A). Moreover, Uro A treatment significantly reduced the number of CD11b/Gr-1–positive MDSCs (Fig. 5B) in pancreatic tumors from PKT mice compared with vehicle-

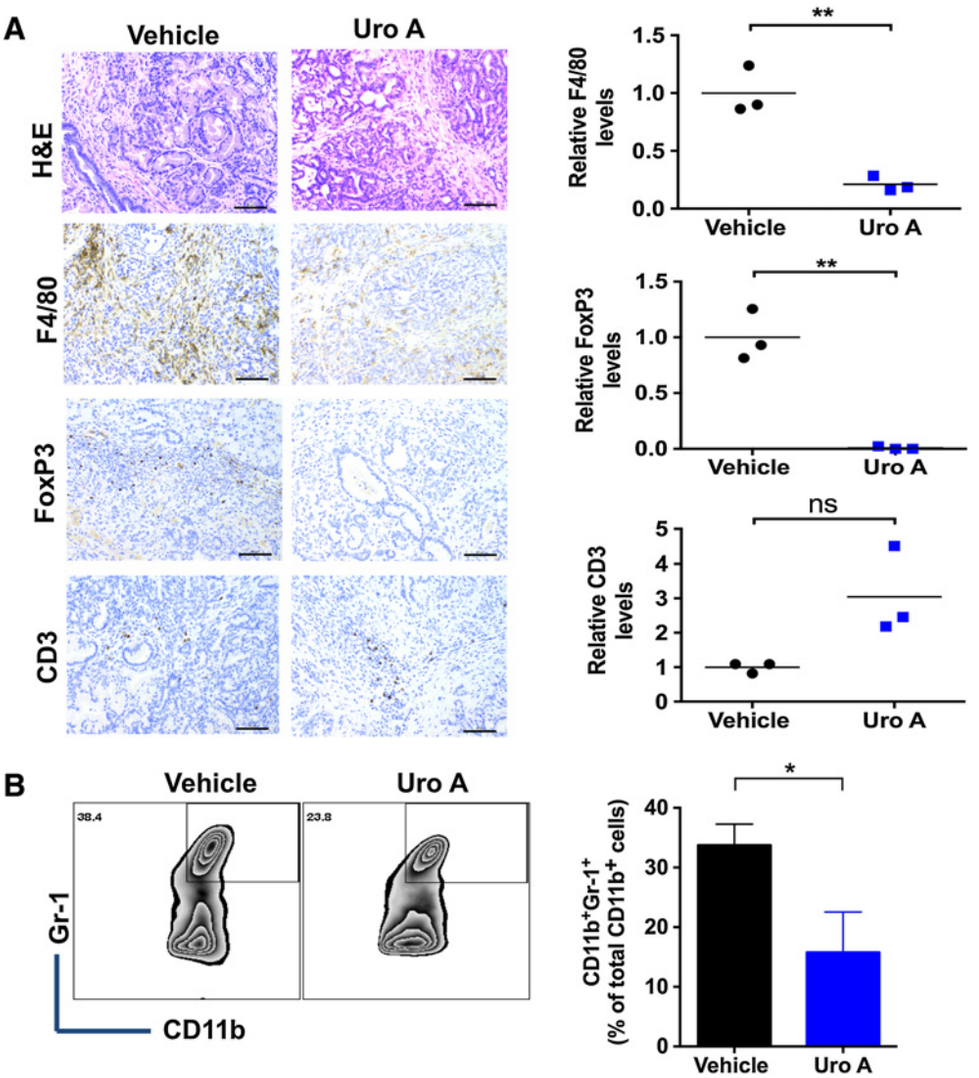

Figure 5.

Effects of Uro A on TAMs, Tregs, and MDSCs in PKT mice. **A,** Representative H&E, F4/80, FoxP3, and CD3 staining of pancreatic tissues harvested from Uro A–treated PKT mice (left plot). Scale bar, 50 μm. Quantification of relative levels of F4/80, FoxP3, and CD3 IHC staining of Uro A and vehicle-treated PKT mice pancreata (right plot; $n = 3$). **B,** Representative flow cytometry zebra plots (left plot) and their corresponding bar graphs (right plot) of MDSCs in the single suspensions of vehicle or Uro A–treated PKT mice pancreata ($n = 3$). *, $P < 0.05$; **, $P < 0.01$ and ns, $P > 0.05$.

treated controls. These findings confirmed that Uro A affected the immune cell population within the tumor, which was coincident with reduced PDAC tumor growth and improved survival.

Discussion

The PI3K/AKT family is among the most frequently mutated pathways in human cancer (32). In a retrospective analysis of patients treated across multiple early phase clinical trials, *PIK3CA*-mutant cancers were shown to have an increased response rate to PI3K/AKT/mTOR pathway inhibitors (33, 34). The PI3K signaling pathway is a downstream effector of oncogenic KRAS (35), which is nearly ubiquitous in PDAC. Aberrant activation of the AKT pathway is commonly associated with tumor initiation, disease progression, and the development of chemotherapeutic resistance (32). A recent study which analyzed all 32 cancer types in The Cancer Genome Atlas (TCGA) has identified several genes (including *Myc* and *KRAS*) which exert a strong protumorigenic effect through PI3K/AKT/mTOR pathway activation in numerous human malignancies, including PDAC (32). TCGA analysis showed that the PI3K/AKT/mTOR pathway is overactivated in *KRAS*-mutant cancers, suggesting that targeting this pathway may even be far more effective in PDAC than other non–*KRAS*-mutant cancers. Furthermore, aberrant activation of the PI3K/AKT signaling pathway results in a subsequent activation of the downstream effector, p70S6 kinase (p70S6K), which primes the ribosome for protein synthesis (35, 36). Once active, AKT regulates cell growth, proliferation, and survival by phosphorylating a variety of downstream antiapoptotic and cell-cycle–related proteins as well as transcription factors (37). Inhibition of the mTORC1 activity loop (i.e., p70S6K at T421/S424) alone is ineffective due to the enhanced activation of the PI3K axis due to loss of mTOR-p70S6K–negative feedback (38). Therefore, identifying a drug capable of targeting both mTOR and PI3K is necessary to avoid pathway reactivation (24, 32). To this end, dual PI3K/mTOR inhibitors are increasingly being considered for clinical use. Our results demonstrate that Uro A effectively inhibits simultaneous PI3K/AKT and mTOR activation in PDAC cells and prevents pathway reactivation both *in vitro* and *in vivo*. This pathway inhibition effectively reduced tumor growth, proliferation, and migration *in vitro*, while it significantly improved OS in the genetically engineered PKT mouse model of PDAC (refs. 35, 36; Fig. 6). These results establish a mechanistic rationale for PI3K/AKT inhibition with Uro A as a potential adjunctive therapy in the treatment of PDAC, for which few effective treatments are currently available.

Uro A is known to mediate its antitumor activities through downregulation of Wnt and IGF-1 signaling in colon and prostate cancer cells (39, 40). Our findings show that, in PDAC, Uro A mediates its antitumor activities through downregulation of PI3K/AKT/mTOR signaling and its downstream targets such as GSK-3β and 4E-BP1, disrupting both tumor cell proliferation and the recruitment of immunosuppressive cells. We posit that therapeutic targeting of the PI3K pathway with its downstream targets AKT and mTOR at multiple levels, as seen from our studies with Uro A, provides better antitumor effects than selective inhibition of a single component of the pathway. We demonstrated that Uro A administration inhibits PDAC cell proliferation through G_1-phase cell-cycle suppression and induction of apoptosis in a dose-dependent manner. These results are in accordance with recent studies where it was shown that Uro A exhibited a significant reduction of cells in G_0–G_1 phase through downregulation of cell-cycle genes such as CCNB1 and CCNB1/P1 in Caco-2 cells (8). Furthermore, our results show that Uro A has minimal impact on normal pancreatic epithelial cells such as HPNE and HPNE-KRAS (Fig. 2F), is well-tolerated, and exerts its antitumor effect at a physiologically appropriate dose. Murine models showed no weight loss or toxic side effects at dose of 20 mg/kg, which is within the range of the concentration of plasma Uro A seen after consumption of EA rich foods.

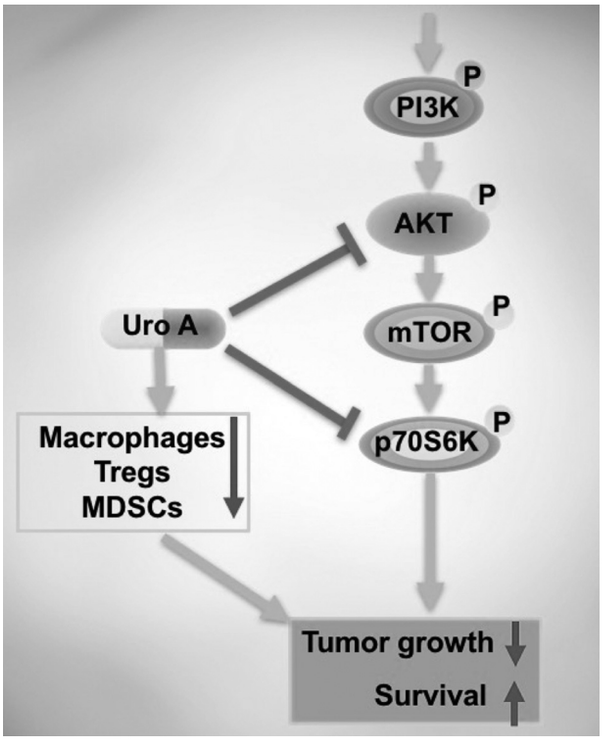

Figure 6.
Biological schematic demonstrating that Uro A intercedes its antitumor effects by targeting PI3K/AKT/mTOR kinase pathways. In addition, Uro A acts on macrophages, Tregs, and MDSCs and thus inhibits tumor growth which enhances survival.

A phase I clinical trial of Uro A demonstrated that it is well-tolerated with good bioavailability (11). Unlike its dietary precursors, ellagitannins, and EA, Uro A is rapidly absorbed and reaches peak plasma concentration 2 hours after ingestion (41). These features make it an ideal candidate for adjunctive dietary interventions for patients with PDAC. In addition to examining its effects as a single-therapy regimen, we also tested whether Uro A could enhance the cytotoxic effects of gemcitabine, the FDA-approved mainstay of PDAC treatment. Our results show combined administration of Uro A and gemcitabine did not provide any survival advantage over monotherapy with Uro A alone. These results could be due to plausible reactivation of resistance pathways such as cyclic AMP response element binding protein (CREB; Supplementary Fig. S3). In our previous studies, we have shown that CREB is a critical regulator of PDAC progression (42), and future studies based on combination of Uro A and a CREB inhibitor may help in further improving the OS for PDAC. Overall, the relative

superiority of Uro A to gemcitabine in our preclinical study highlights the need to study Uro A as a chemopreventive agent and pursue Uro A treatment in clinical trials versus gemcitabine.

PDAC is generally considered an immunologically cold tumor wherein the immunosuppressive milieu (comprised of MDSCs, TAMs, and Tregs) limits the activity of chemotherapeutic agents and blunts the host immune response (43, 44). These protumorigenic immune cells play a major role in promoting disease progression and/or drug resistance and hence have become a major focus of targeted therapeutics. Our results demonstrated an increase in the accumulation of MDSCs in untreated PDAC tumors, which could be attributed to an excess of proinflammatory factors within the TME. Uro A treatment effectively suppressed infiltration of MDSCs as well as Tregs and TAMs, suggesting that Uro A in part limits immunosuppression in PDAC (Fig. 5).

Collectively, our study demonstrated that the natural compound Uro A inhibited the PI3K/AKT/mTOR pathway and induced a strong antiproliferative and proapoptotic effect both *in vitro* and *in vivo*. Uro A monotherapy significantly improved survival, providing evidence for its potential as a promising therapeutic approach in PDAC treatment. Given that dual PI3K/mTOR inhibitors are increasingly being considered for clinical use, the findings presented here suggest the potential use of Uro A, a natural, well-tolerated compound which is a potent inhibitor of the PI3K/mTOR pathway, as a novel treatment option in PDAC.

Disclosure of Potential Conflicts of Interest

No potential conflicts of interest were disclosed.

Authors' Contributions

Conception and design: T.M. Totiger, S. Srinivasan, V.R. Jala, P. Lamichhane, A.R. Dosch, P.K. Vemula, M. VanSaun, N.B. Merchant, N.S. Nagathihalli
Development of methodology: T.M. Totiger, S. Srinivasan, P. Lamichhane, M. VanSaun, N.B. Merchant, N.S. Nagathihalli
Acquisition of data (provided animals, acquired and managed patients, provided facilities, etc.): T.M. Totiger, S. Srinivasan, P. Lamichhane, A.R. Dosch, C. Joshi, S. Rangappa, J. Castellanos, N. Kashikar, N.S. Nagathihalli
Analysis and interpretation of data (e.g., statistical analysis, biostatistics, computational analysis): T.M. Totiger, S. Srinivasan, P. Lamichhane, A.R. Dosch, A.A. Gaidarski III, S. Rangappa, J. Castellanos, X. Chen, D. Kwon, M. VanSaun, N.B. Merchant, N.S. Nagathihalli
Writing, review, and/or revision of the manuscript: S. Srinivasan, V.R. Jala, P. Lamichhane, A.R. Dosch, A.A. Gaidarski III, C. Joshi, D. Kwon, N. Kashikar, M. VanSaun, N.B. Merchant, N.S. Nagathihalli
Administrative, technical, or material support (i.e., reporting or organizing data, constructing databases): T.M. Totiger, S. Srinivasan, P.K. Vemula, M. VanSaun, N.S. Nagathihalli
Study supervision: N.S. Nagathihalli

Acknowledgments

The authors thank Dr. Xizi Dai, Dr. Kumaraswamy Honnenahally, and Yanhua Xiong for their technical and administrative assistance.

This work was supported by the NIH NCI R21 CA209536, American Cancer Society IRG 98-277-13, and Stanley Glaser Foundation Research Award (UM SJG 2017-24) to N.S. Nagathihalli, R01 CA161976 and NIH T32 CA211034 to N.B. Merchant, and NCI R21 CA216090 to V.R. Jala. Histopathology Core Service was performed through the Sylvester Comprehensive Cancer Center (SCCC) support grant (N.S. Nagathihalli).

The costs of publication of this article were defrayed in part by the payment of page charges. This article must therefore be hereby marked *advertisement* in accordance with 18 U.S.C. Section 1734 solely to indicate this fact.

Received May 1, 2018; revised September 6, 2018; accepted October 29, 2018; published first November 7, 2018.

References

1. Siegel RL, Miller KD, Jemal A. Cancer statistics, 2016. CA Cancer J Clin 2016;66:7–30.
2. Ryan DP, Hong TS, Bardeesy N. Pancreatic adenocarcinoma. N Engl J Med 2014;371:2140–1.
3. Fokas E, O'Neill E, Gordon-Weeks A, Mukherjee S, McKenna WG, Muschel RJ. Pancreatic ductal adenocarcinoma: from genetics to biology to radiobiology to oncoimmunology and all the way back to the clinic. Biochim Biophys Acta 2015;1855:61–82.
4. Atanasov AG, Waltenberger B, Pferschy-Wenzig EM, Linder T, Wawrosch C, Uhrin P, et al. Discovery and resupply of pharmacologically active plant-derived natural products: A review. Biotechnol Adv 2015;33:1582–614.
5. Newman DJ, Cragg GM. Natural products as sources of new drugs from 1981 to 2014. J Nat Prod 2016;79:629–61.
6. Patridge E, Gareiss P, Kinch MS, Hoyer D. An analysis of FDA-approved drugs: natural products and their derivatives. Drug Discov Today 2016;21:204–7.
7. Veeraraghavan J, Natarajan M, Lagisetty P, Awasthi V, Herman TS, Aravindan N. Impact of curcumin, raspberry extract, and neem leaf extract on rel protein-regulated cell death/radiosensitization in pancreatic cancer cells. Pancreas 2011;40:1107–19.
8. Gonzalez-Sarrias A, Espin JC, Tomas-Barberan FA, Garcia-Conesa MT. Gene expression, cell cycle arrest and MAPK signalling regulation in Caco-2 cells exposed to ellagic acid and its metabolites, urolithins. Mol Nutr Food Res 2009;53:686–98.
9. Cheng H, Lu C, Tang R, Pan Y, Bao S, Qiu Y, et al. Ellagic acid inhibits the proliferation of human pancreatic carcinoma PANC-1 cells in vitro and in vivo. Oncotarget 2017;8:12301–10.
10. Lei F, Xing DM, Xiang L, Zhao YN, Wang W, Zhang LJ, et al. Pharmacokinetic study of ellagic acid in rat after oral administration of pomegranate leaf extract. J Chromatogr B Analyt Technol Biomed Life Sci 2003;796:189–94.
11. Heilman J, Andreux P, Tran N, Rinsch C, Blanco-Bose W. Safety assessment of Urolithin A, a metabolite produced by the human gut microbiota upon dietary intake of plant derived ellagitannins and ellagic acid. Food Chem Toxicol 2017;108:289–97.
12. Gossage L, Eisen T. Targeting multiple kinase pathways: a change in paradigm. Clin Cancer Res 2010;16:1973–8.
13. Tomas-Barberan FA, Gonzalez-Sarrias A, Garcia-Villalba R, Nunez-Sanchez MA, Selma MV, Garcia-Conesa MT, et al. Urolithins, the rescue of "old" metabolites to understand a "new" concept: metabotypes as a nexus among phenolic metabolism, microbiota dysbiosis, and host health status. Mol Nutr Food Res 2017;61.
14. Garrido-Laguna I, Hidalgo M. Pancreatic cancer: from state-of-the-art treatments to promising novel therapies. Nat Rev Clin Oncol 2015;12:319–34.
15. Oettle H, Post S, Neuhaus P, Gellert K, Langrehr J, Ridwelski K, et al. Adjuvant chemotherapy with gemcitabine vs observation in patients undergoing curative-intent resection of pancreatic cancer: a randomized controlled trial. JAMA 2007;297:267–77.
16. Saha P, Yeoh BS, Singh R, Chandrasekar B, Vemula PK, Haribabu B, et al. Gut microbiota conversion of dietary ellagic acid into bioactive phytoceutical urolithin a inhibits heme peroxidases. PLoS One 2016;11:e0156811.
17. Nagathihalli NS, Beesetty Y, Lee W, Washington MK, Chen X, Lockhart AC, et al. Novel mechanistic insights into ectodomain shedding of EGFR Ligands Amphiregulin and TGF-alpha: impact on gastrointestinal cancers driven by secondary bile acids. Cancer Res 2014;74:2062–72.
18. Nagathihalli NS, Castellanos JA, Shi C, Beesetty Y, Reyzer ML, Caprioli R, et al. Signal transducer and activator of transcription 3, mediated remodeling of the tumor microenvironment results in enhanced tumor drug delivery in a mouse model of pancreatic cancer. Gastroenterology 2015;149:1932–43.

19. Deer EL, Gonzalez-Hernandez J, Coursen JD, Shea JE, Ngatia J, Scaife CL, et al. Phenotype and genotype of pancreatic cancer cell lines. Pancreas 2010;39:425–35.
20. Ijichi H, Chytil A, Gorska AE, Aakre ME, Fujitani Y, Fujitani S, et al. Aggressive pancreatic ductal adenocarcinoma in mice caused by pancreas-specific blockade of transforming growth factor-beta signaling in cooperation with active Kras expression. Genes Dev 2006;20:3147–60.
21. Wu J, Houghton PJ. Interval approach to assessing antitumor activity for tumor xenograft studies. Pharm Stat 2010;9:46–54.
22. Nunez-Sanchez MA, Garcia-Villalba R, Monedero-Saiz T, Garcia-Talavera NV, Gomez-Sanchez MB, Sanchez-Alvarez C, et al. Targeted metabolic profiling of pomegranate polyphenols and urolithins in plasma, urine and colon tissues from colorectal cancer patients. Mol Nutr Food Res 2014;58:1199–211.
23. Espin JC, Larrosa M, Garcia-Conesa MT, Tomas-Barberan F. Biological significance of urolithins, the gut microbial ellagic Acid-derived metabolites: the evidence so far. Evid Based Complement Alternat Med 2013;2013:270418.
24. Engelman JA. Targeting PI3K signalling in cancer: opportunities, challenges and limitations. Nat Rev Cancer 2009;9:550–62.
25. Zoncu R, Efeyan A, Sabatini DM. mTOR: from growth signal integration to cancer, diabetes and ageing. Nat Rev Mol Cell Biol 2011;12:21–35.
26. Dienstmann R, Rodon J, Serra V, Tabernero J. Picking the point of inhibition: a comparative review of PI3K/AKT/mTOR pathway inhibitors. Mol Cancer Ther 2014;13:1021–31.
27. Clark CE, Beatty GL, Vonderheide RH. Immunosurveillance of pancreatic adenocarcinoma: insights from genetically engineered mouse models of cancer. Cancer Lett 2009;279:1–7.
28. Bayne Lauren J, Beatty Gregory L, Jhala N, Clark Carolyn E, Rhim Andrew D, Stanger Ben Z, et al. Tumor-derived granulocyte-macrophage colony-stimulating factor regulates myeloid inflammation and T cell immunity in pancreatic cancer. Cancer Cell 2012;21:822–35.
29. Fontenot JD, Rudensky AY. A well adapted regulatory contrivance: regulatory T cell development and the forkhead family transcription factor Foxp3. Nat Immunol 2005;6:331–7.
30. Mills CD, Kincaid K, Alt JM, Heilman MJ, Hill AM. M-1/M-2 macrophages and the Th1/Th2 paradigm. J Immunol 2000;164:6166–73.
31. Huijts CM, Santegoets SJ, Quiles Del Rey M, de Haas RR, Verheul HM, de Gruijl TD, et al. Differential effects of inhibitors of the PI3K/mTOR pathway on the expansion and functionality of regulatory T cells. Clin Immunol 2016;168:47–54.
32. Zhang Y, Kwok-Shing Ng P, Kucherlapati M, Chen F, Liu Y, Tsang YH, et al. A pan-cancer proteogenomic atlas of PI3K/AKT/mTOR pathway alterations. Cancer Cell 2017;31:820–32e3.
33. Janku F, Wheler JJ, Naing A, Falchook GS, Hong DS, Stepanek VM, et al. PIK3CA mutation H1047R is associated with response to PI3K/AKT/mTOR signaling pathway inhibitors in early-phase clinical trials. Cancer Res 2013;73:276–84.
34. Samuels Y, Wang Z, Bardelli A, Silliman N, Ptak J, Szabo S, et al. High frequency of mutations of the PIK3CA gene in human cancers. Science 2004;304:554.
35. Shaw RJ, Cantley LC. Ras, PI(3)K and mTOR signalling controls tumour cell growth. Nature 2006;441:424–30.
36. Wong MH, Xue A, Baxter RC, Pavlakis N, Smith RC. Upstream and downstream co-inhibition of mitogen-activated protein kinase and PI3K/Akt/mTOR pathways in pancreatic ductal adenocarcinoma. Neoplasia 2016;18:425–35.
37. Manning BD, Cantley LC. AKT/PKB signaling: navigating downstream. Cell 2007;129:1261–74.
38. O'Reilly KE, Rojo F, She QB, Solit D, Mills GB, Smith D, et al. mTOR inhibition induces upstream receptor tyrosine kinase signaling and activates Akt. Cancer Res 2006;66:1500–8.
39. Sharma M, Li L, Celver J, Killian C, Kovoor A, Seeram NP. Effects of fruit ellagitannin extracts, ellagic acid, and their colonic metabolite, urolithin A, on Wnt signaling. J Agric Food Chem 2010;58:3965–9.
40. Vicinanza R, Zhang Y, Henning SM, Heber D. Pomegranate juice metabolites, ellagic acid and urolithin a, synergistically inhibit androgen-independent prostate cancer cell growth via distinct effects on cell cycle control and apoptosis. Evid Based Complement Alternat Med 2013;2013:247504.
41. Seeram NP, Aronson WJ, Zhang Y, Henning SM, Moro A, Lee RP, et al. Pomegranate ellagitannin-derived metabolites inhibit prostate cancer growth and localize to the mouse prostate gland. J Agric Food Chem 2007;55:7732–7.
42. Srinivasan S, Totiger T, Shi C, Castellanos J, Lamichhane P, D'osch RA, et al. Tobacco carcinogen-induced production of GM-CSF activates CREB to promote pancreatic cancer. Cancer Res 2018;78:6146–58.
43. Takeuchi S, Baghdadi M, Tsuchikawa T, Wada H, Nakamura T, Abe H, et al. Chemotherapy-derived inflammatory responses accelerate the formation of immunosuppressive myeloid cells in the tissue microenvironment of human pancreatic cancer. Cancer Res 2015;75:2629–40.
44. Winograd R, Byrne KT, Evans RA, Odorizzi PM, Meyer AR, Bajor DL, et al. Induction of T-cell immunity overcomes complete resistance to PD-1 and CTLA-4 blockade and improves survival in pancreatic carcinoma. Cancer Immunol Res 2015;3:399–411.